ACS APPLIED POLYMER MATERIALS

pubs.acs.org/acsapm Article

Nanocellulose and Elastin Act as Plasticizers of Electrospun Bioinspired Scaffolds

Nicola Ciarfaglia, Antonietta Pepe, Germano Piccirillo, Antonio Laezza, Ruben Daum, Katja Schenke-Layland, and Brigida Bochicchio*

Cite This: ACS Appl. Polym. Mater. 2020, 2, 4836−4847 Read Online

ACCESS | Metrics & More | Article Recommendations | Supporting Information

ABSTRACT: In this work, we produced cross-linked electrospun hybrid scaffolds composed of gelatin/poly-D,L-lactide (PDLLA), gelatin/PDLLA/nanocellulose, and gelatin/PDLLA/cellulose nanocrystals/elastin. Fourier-transform infrared spectroscopy, X-ray diffraction, and high-performance liquid chromatography demonstrated the complete embedding of each component in the hybrid scaffolds. The degree of cross-linking was quantified by the 2,4,6-trinitrobenzenesulfonic acid assay, and attenuated total reflectance spectroscopy revealed the effectiveness of the cross-linking reaction. Notably, the interconnected porous structure revealed in uncross-linked scaffolds persisted even after cross-linking. Scaffolds were characterized in water through their contact angle showing total wettability. We investigated their mechanical properties by uniaxial tensile testing, which showed that even in the dry state, nanocellulose- and elastin-containing scaffolds exhibit higher elongation at rupture compared to those with pure gelatin/PDLLA. Therefore, we succeeded in tuning the toughness of the scaffolds by modulating the composition. In order to use scaffolds as medical devices, we assayed fibroblasts on scaffold extraction media, indicating that they were noncytotoxic. Finally, the attachment and proliferation of fibroblasts on the surface of different scaffolds were evaluated.

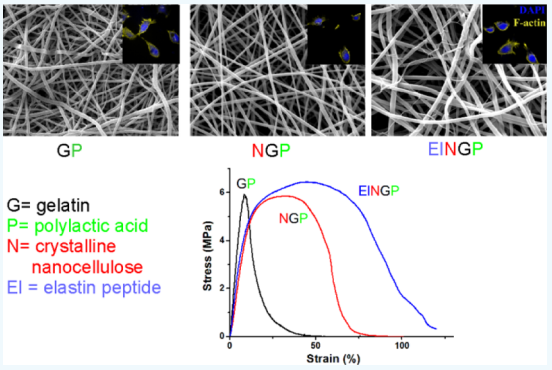

KEYWORDS: *elastin, cellulose nanocrystals, electrospinning, cell attachment, proliferation, plasticity*

INTRODUCTION

Electrospinning has been employed for the production of materials composed of nano- and micro-structured nonwoven tissues, with applications ranging from electrode production[1] and catalysis[2,3] to drug delivery, tissue engineering,[4−7] and biosensing.[8,9]

Pore connectivity and the high ratio between the surface and the area of fibers mark electrospun polymers as high-performing materials,[4] especially in drug delivery and tissue engineering applications as they mimic the complexity and three-dimensional size of the extracellular matrix (ECM) acting as a physical support for anchoring cells that would regenerate new tissues after injury and damage.[10−12] Afterward, the scaffold would degrade to byproducts in the form of metabolites according to a property called bioresorbability.[13]

Synthetic polyesters have been widely electrospun into fibrous scaffolds,[14] with poly-ε-caprolactone (PCL) and polyglycolic acid as well-known examples. Besides, polylactic acid (PLA) is one of the most used polymers in biomedical applications because of its biocompatibility and biodegradability.[15,16] It degrades to lactic acid, its monomeric unit, a metabolite produced in mammalian muscles during glycogenolysis.[17] It can be commercially produced either from petrochemical feedstock or from bacterial sources affording a racemic and enantiomerically pure polymer.[18−25] However, the main disadvantages in the use of PLA are related to its slow degradation rate, hydrophobicity, and brittleness.[26]

Enantiomeric pure forms of PLA[27,28] are semicrystalline polymers, whereas the raceme poly-D,L-lactide (PDLLA) has a lower crystalline degree and shows a faster degradation rate. Notably, the degradation rate is a function of molecular weight and crystallinity degree: the higher the crystallinity, the higher the degradation times.[26] On this basis, PDLLA has been preferred to poly-L-lactide (PLLA) for electrospun matrices in bone regeneration.[29] However, one of the main weaknesses in the use of PDLLA is its strong hydrophobicity.[30] In order to overcome these drawbacks, hydrophilic and natural polymers were added as complementary components to PDLLA.

Gelatin (GE), for example, is highly biocompatible and biodegradable and has the ability to promote cell adhesion and accelerate the wound-healing process.[31] The use of GE fulfills a

Received: July 21, 2020
Accepted: October 21, 2020
Published: October 30, 2020

https://dx.doi.org/10.1021/acsapm.0c00790
ACS Appl. Polym. Mater. 2020, 2, 4836−4847

Table 1. Scaffold Composition

abbreviation[a]	polymer weight ratio	final % (w/v)	final volume (mL)
GP	GE/PDLLA = 1:3	12.0	3.0
NGP	CNCs/GE/:PDLLA = 1:3:9	13.0	3.0
ElNGP	EX15/CNCs/GE/PDLLA = 1:7.5:22.5:67	13.1	3.0

[a]GP: (gelatin/poly-lactic acid), NGP: (cellulose nanocrystals/gelatin/poly-lactic acid), ElNGP: (EX15 elastin-like peptide/cellulose nanocrystals/gelatin/poly-lactic acid).

double issue: increasing the hydrophilicity of the scaffolds and inserting bioactive sequences. Besides GE, other proteins are blended with synthetic polymers. Human recombinant tropoelastin, for example, has been successfully electrospun with poly(ethylene glycol) (PEG).[32] Elastin (El) is a cross-linked polymer whose insolubility hampers the study of its molecular structure in solution. Short El peptides encoded by single exons of human tropoelastin gene (HTE) were easily investigated, revealing the structure−function relationship of the entire protein. One of the most appealing peptides was the sequence encoded by exon 15 (EX15) of HTE, which is considered bioactive (data not shown) and having GVGPQAAAAAAAKAAAKF as the primary structure.[33]

To overcome the unfit performances of PLA-based scaffolds' mechanical trials and improve their biomedical applications, nanoparticle composites with metallic[34,35] and cellulose nanofillers have been developed.[36]

Cellulose nanocrystals (CNCs) are gaining increasing interest as nanofillers in the perspective of employing renewable resources which are preferable to oil-based polymers in terms of sustainability.[37] They are mainly produced by acid hydrolysis of cellulose, with dimensions dependent on the sources and hydrolysis conditions employed[38,39] and exhibit estimated Young's modulus and tensile strength of 138 GPa and 7500 MPa, respectively, in the crystalline region.[40] The use of CNCs allowed tuning the tensile strength, strain, Young's modulus, and toughness in PLA/CNCs/PEG composites[41] as well as they are reported for polyvinyl alcohol films in the presence of 1,2,3,4-butane tetracarboxylic acid as a cross-linking agent.[42]

In the present work, we have combined for the first time El peptides, CNCs, GE, and PDLLA for the production of electrospun membranes obtaining noncytotoxic scaffolds with fiber diameters and mechanical properties appealing for the development of new wound-dressing materials. The problems common to conventional dressings are that they do not ensure a moist environment, and moreover, they adhere to desiccated wound surfaces causing trauma upon removal. Besides, severe wound dehydration would disturb the ideal moist healing environment and delay wound healing.[43] The aim of the present work was to obtain hydrophilic wound dressings by modulating the scaffold composition through the addition of biopolymers that are able to maintain a moist environment at the wound interface. PDLLA and GE alone are ineffective as dressing materials; therefore, both polymers were blended together and along with El and nanocellulose serve as a suitable wound dressing material from mechanical and biological points of view.

EXPERIMENTAL SECTION

Materials and Methods. Commercial-grade reagents and solvents were used without further purification, except where otherwise indicated.

Electrospinning. GE from bovine skin (type B powder, bloom strength: 225, isoelectric point: 3.8−5.5 at 25 °C) was purchased from Sigma-Aldrich (St. Louis, Missouri, USA). PDLLA (EasyFil PLA, transparent pellets, molecular weight: 126,000 g/mol, density: 1240 kg/m^3) was obtained from FormFutura (Nijmegen, Netherlands). CNCs (from wood, spray-dried powder, particle size: 1−50 μm, particle length: 44−108 nm, particle diameter: 2.3−4.5 nm, pH: 6−7, crystalline fraction: 88%) were bought from CelluForce (Montreal, Quebec, Canada). El peptide was synthesized as reported previously.[33] All the polymers were dissolved in 3 mL of 1,1,1,3,3,3-hexafluoro-2-propanol (HFP) (Iris Biotech GMBH, Marktredwitz, Germany). Polymer solutions were prepared in the ratio percentages listed in Table 1. All mixtures containing GE were prepared at 37 °C by dissolving GE in HFP. The solution was kept under magnetic stirring for 2 h. Afterward, PDLLA was added and the mixture was kept under magnetic stirring for 3 h. The polymer mixture containing CNCs was prepared by adding CNCs previously dispersed in HFP at room temperature and kept under magnetic stirring for 24 h. CNC dispersion underwent different sonication cycles. The polymer mixtures were loaded into a 5 mL plastic syringe with an 18 G stainless-steel needle and then electrospun at 19 kV (Gamma High-Voltage generator), with a flow rate of 1.6 mL/h of the pump for a single syringe BSP-99 mM (Linari Engineering, Pisa, Italy). The target was a round copper plate having 9 mm diameter coated with aluminum foils and the distance between the collector and the needle was set to 19 cm.

Cross-Linking Procedure. *N*-Hydroxysuccinimide (NHS) and *N*-(3-dimethylaminopropyl)-*N*′-ethyl-carbodiimide hydrochloride (EDC·HCl) were used as cross-linking reagents and purchased from Sigma-Aldrich (St. Louis, Missouri, USA) and Novabiochem (Darmstadt, Germany), respectively. Cross-linkers were solubilized in an 85.5% ethanolic solution (Carlo Erba Reagents, Cornaredo, Italy) in an equimolar ratio, both at the concentration of 45.0 mM. Electrospun scaffolds were immersed in a cross-linking solution at room temperature. Subsequently, they were shaken at 60 rpm using an orbital shaker (PSU-10i, Biosan, Riga, Latvia) for 24 h. The electrospun materials were gently dried by using a filter paper and washed with ultrapure water (20 mL × 3 times) to remove any residual trace of cross-linkers. Finally, they were immersed in 95.0% ethanol, shaken again for 1 h at 60 rpm, and air-dried at room temperature. Ultrapure water was produced by a Milli-Q Water Purification System (Merck, Darmstadt, Germany). Water is first pumped through the reverse osmosis cartridge; thereafter, the permeate water is pumped from the reservoir through the Quantum cartridge by the recirculation pump in order to produce high-resistivity product water, which is delivered at a flow rate of 0.6 L/min through a 0.22 μm filter.

Amine Group Content and Degree of Cross-Linking. The content of free primary amine groups present in the uncross-linked scaffolds and that in cross-linked were determined using the 2,4,6-trinitrobenzenesulfonic acid (TNBS) assay with a protocol similar to those reported by Davidenko[44] and Ofner.[45] To each sample (4−6 mg), 0.5 mL of a 4% (w/v) $NaHCO_3$ solution and 0.5 mL of a freshly prepared solution of 0.05% (w/v) TNBS were added. After 2 h at 40 °C, 1.5 mL of 6 M HCl was added and the samples were hydrolyzed at 60 °C for 90 min. The reaction mixture was diluted with distilled water (2.5 mL) and cooled to room temperature, and absorbance at λ = 346 nm was measured using a Cary 60 UV−Vis spectrometer (Agilent, Santa Clara, USA). Controls (blank samples) were prepared using the same procedure, except that HCl was added, prior to the

https://dx.doi.org/10.1021/acsapm.0c00790
ACS Appl. Polym. Mater. 2020, 2, 4836−4847

introduction of the TNBS solution, to prohibit any reaction of TNBS with the amine groups. The blank sample value was subtracted from each sample absorbance. Three replicates on three pieces of each scaffold were used for each determination. The uncross-linked sample was assumed to contain 100% of the available free amine groups and this value was used to calculate the percentage of remaining free amine groups after the cross-linking treatment using the following equation (eq 1)

$$\frac{n(\mathrm{NH_2})}{g(\mathrm{scaffold})} = \frac{(\mathrm{Abs} \times V)}{(14,\,600\ \mathrm{L\ mol^{-1}\ cm^{-1}} \times W \times l)} \quad (1)$$

In the above formula used for the calculation of the amine group content, 14,600 L mol^{-1} cm^{-1} is the molar extinction constant at λ = 346 nm of TNBS-Lys, while V is the volume (L), W is the mass sample (g), and l is the cell path length (cm).

The degree of cross-linking was evaluated as the difference between the chemically determined number of free amine groups before and after cross-linking, relative to the initial free amine content.

X-ray Diffraction Analysis. CNC powder was analyzed by X-ray diffraction (XRD) and used as a standard to characterize electrospun scaffolds containing CNCs. XRD analysis was carried out on a Siemens D5000 diffractometer (Munich, Germany). The current generator and the voltage generator adjusted at 32 mA and 40 kV, respectively, and the step size was kept at 0.042, with a total duration of analysis of 75 min.

High-Performance Liquid Chromatography. Small pieces of uncross-linked and cross-linked ElNGP (EX15/CNCs/GE/PDLLA) hybrid scaffolds (1 cm × 1 cm) were immersed in 85.5% ethanol solution and shaken at 60 rpm using an orbital shaker (PSU-10i, Biosan, Riga, Latvia) for 24 h. Afterward, the solution was transferred into a round-bottom flask, evaporated under nitrogen flow, diluted with ultrapure water, and freeze-dried. After lyophilization, the solid was solubilized in H_2O (0.1% TFA) and analyzed by reverse-phase HPLC on a Jupiter 300 Å C18 analytical column (250 × 4.60 μm 5 Å) (Phenomenex, Bologna, Italy). H_2O (0.1% TFA) and CH_3CN (0.1% TFA) in a 95:5 ratio, respectively, were used as mobile phases in the binary gradient. The uncross-linked ElNGP scaffold was immersed in 85.5% ethanol solution of EDC/NHS (45 mM). The solution was shaken at 60 rpm for 24 h, treated as previously described, and analyzed by HPLC. EX15 El-inspired peptide was used as standard and analyzed by HPLC in both aqueous and cross-linking solutions.

Fourier-Transform Infrared Spectroscopy. FTIR spectroscopy was performed in the solid state in KBr pellets using a Jasco FTIR 460 plus (JASCO, Easton, MD, USA) spectrometer in order to analyze electrospun scaffolds. Contextually, pure polymers GE, CNCs, and PDLLA were processed and used as reference. Each electrospun scaffold was cut into small pieces and added to KBr powder previously dried under vacuum at 180 °C for 12 h. Spectra were acquired in the region from 4000 to 500 cm^{-1} using 256 scans and a resolution of 2 cm^{-1}. The KBr pellet spectrum was recorded before each measurement and then subtracted from the sample spectrum.

Attenuated Total Reflectance. Attenuated total reflectance (ATR) spectra were obtained out on electrospun scaffolds before and after the cross-linking reaction. Measurements were carried out on a Nicolet 5700 (Thermo Fisher Scientific, Waltham, MA, USA) equipped with an ATR accessory, Smart Orbit with a type II A diamond crystal, of refractive index 2.4, with a KBr beam splitter and an MCT/B detector. Spectra were acquired in the region from 4000 to 450 cm^{-1} with a spectral resolution of 2 cm^{-1} and 32 scans. Background spectra were recorded each time and then subtracted from the sample spectra.

Scanning Electron Microscopy. The morphology of the electrospun scaffolds was investigated on a Philips, FEI ESEM XL30 instrument. SEM images were acquired with a voltage of 20 kV and different magnifications, after gold sputter-coating. The diameter of the fibers and scaffold porosity were evaluated using ImageJ (National Institute of Health, USA, http://rsbweb.nih.gov/ij) software supplied with the DiameterJ plug-in (n > 1000).

Swelling Test Analysis. For each sample, four pieces from four different cross-linked scaffolds (a total of 16 samples) were investigated. Each sample was immersed in 10 mL of ddH_2O at room temperature (r.t.) for 60 min and shaken at 60 rpm on an orbital shaker. Thereafter, they were gently dried on a filter paper to remove the excess of water and weighed on a balance (Precisa Instruments AG, Model, XR 205 SM-DR, 8953 Dietikon, Switzerland, 2005) having a sensitivity of ±0.00001 g. The water absorbed by each scaffold was calculated according to the following equation (eq 2)

$$\mathrm{swelling}\ (\%) = \frac{W_w - W_d}{W_d} \times 100 \quad (2)$$

In the above formula used for the swelling test, W_w and W_d are the masses (g) of wet and dry scaffolds, respectively.

Contact Angle Measurements. An indirect evaluation of the hydrophilicity scaffold was assessed by the contact angle on an OCA 40 device (DataPhysics Instruments GmbH, Filderstadt, Germany) instrument. The final result is calculated from 16 measurements obtained from four different pieces for each cross-linked scaffold. A water drop having 2 μL of volume was placed onto the sample and after 10 s the contact angle was measured using a video setup and SCA20 software (DataPhysics Instruments).

Uniaxial Tensile Testing. For each sample, four rectangular pieces from four different cross-linked scaffolds were obtained (10 mm × 20 mm). They were clamped to the uniaxial tensile testing device (ElectroForce 5500, ElectroForce Systems Group, Bose Corporation, Minnesota, USA). They were pulled to failure after applying a stretch of 0.025 mm s^{-1}. Then, Young's modulus and the ultimate tensile strength were calculated. For each measurement, E modulus was calculated using the initial linear slope of the stress versus strain curve.

Cytotoxicity Assay. Prior to cell culture experiments, the fabricated scaffolds were tested for biocompatibility. For this purpose, a cytotoxicity test according to EN ISO 10993-5 has been performed using the MTS assay CellTiter 96 AQueous OneSolution Cell Proliferation Assay (G3582, Promega, Madison, USA). Each polymer was incubated for 72 h at 37 °C and 5% CO_2 in Dulbecco's modified Eagle's medium (21063-029, Thermo Fisher Scientific, Waltham, USA) and 1% penicillin−streptomycin (15070-063, Thermo Fisher Scientific) in an extraction ratio of 0.1 g/mL. NIH/3T3 cells (ATCC CRL-1658TM, ATCC, Manassas, USA) were then cultured for 24 h with the sterile filtered extraction medium supplemented with 10% fetal bovine serum (10270-106, Thermo Fisher Scientific). The medium without polymer extract served as a negative control. The cells incubated with 1% SDS were used as a positive control. Subsequently, the MTS assay was performed according to the manufacturer's protocol. The absorbance of the soluble formazan produced by the cellular reduction of MTS was measured at 490 nm (n = 3). The cell viability was determined by the absorption of the samples relative to the control.

Cell Seeding and Culture on the Electrospun Scaffolds. In order to investigate cell attachment and proliferation, L929 cells (ACC2, Leibniz Institute DSMZ, Braunschweig, Germany) were cultured onto the scaffolds for 1, 3, and 5 days (n = 3). Briefly, scaffolds with a diameter of 6 mm were placed in a 96-well plate and 5000 cells/mL were seeded in 150 μL of modified Eagle's medium (11090081, Thermo Fisher Scientific) supplemented with 4 mM L-glutamine (A2916801, Thermo Fisher Scientific), 1% penicillin−streptomycin, and 10% fetal bovine serum. Cells were cultured at 37 °C and 5% CO_2. The medium was changed every 2 days. After cell culture, the cell-seeded scaffolds were washed once with PBS and fixed with 4% paraformaldehyde (P6148, Sigma-Aldrich). The cell membrane was permeabilized with 0.1% Triton X-100 (3051.3, Carl Roth, Karlsruhe, Germany) for 20 min. F-actin was stained for 30 min in the dark using Alexa Fluor 647 (1:500, A22287, Thermo Fisher Scientific). For cell number analysis, the cells were stained with 4′,6-diamidino-2-phenylindole (DAPI) (1:50, 10236276001, Roche Diagnostics, Mannheim, Germany) for 20 min. Images were obtained using a fluorescence microscope (Cell Observer, Carl Zeiss AG,

https://dx.doi.org/10.1021/acsapm.0c00790
ACS Appl. Polym. Mater. 2020, 2, 4836−4847

Oberkochen, Germany). The cell number was quantified by counting the DAPI-stained cell nuclei per area using ImageJ.[46]

Statistical Analysis. The graphs were plotted using Origin Data Graph software (OriginLab Corporation, Northampton, MA, USA) and Microsoft Excel. Data are reported as mean ± standard deviation. Fiber diameter and swelling test statistical analyses were carried out using the one-way analysis of variance (ANOVA) method, Tukey's test, and Student's *t*-test. A p value ≤ 0.01 (*) was considered as statistically significant. For the porosity and mechanical analysis, two-way analysis of variance and Tukey's test were used, with a p value ≤ 0.05 (*) defined as statistically significant, while for the cytotoxicity assay ANOVA was performed and the mean value of the samples was compared with the mean value of the negative control using Fisher's least significant difference test. For cell number analysis, a two-way ANOVA and Tukey's multiple comparison test were performed with GraphPad PRISM (GraphPad Software, San Diego, USA).

RESULTS AND DISCUSSION

Production of Electrospun Scaffolds. Starting from the first application,[47] nowadays electrospinning has gained even more diffusion for the production of scaffolds in tissue engineering.[48,49] Our work aimed to produce electrospun scaffolds made of natural polymers such as cellulose, protein-based materials, and PDLLA. Recently, recombinant HTE has been electrospun with collagen to improve biocompatibility of scaffolds.[50] Herein, an El-derived peptide with a bioactive sequence was added to the polymer mixture. CNCs are generally used to reinforce scaffolds electrospun from different polymers, such as—polyvinylidenefluoride-*co*-hexafluoropropylene (PVDF-HFP),[51] PCL,[52] polyacrylonitrile (PAN),[53] and PLA.[54]

In the present study, CNCs were added to counterbalance the strong hydrophobicity of PDLLA and improve the mechanical properties of hybrid scaffolds. Polymer solutions described in Table 1 were electrospun using process parameters recently published elsewhere.[55]

HFP, known for its low nucleophilicity and strong hydrogen bond-donating ability,[56,57] was chosen as a solvent because of its ability to solubilize proteins, PLA polymer,[55] GE, El, and CNCs, even if in the final form of a dispersion. The GP blend (GE/PDLLA) was prepared by mixing GE and PDLLA to a final concentration of 3.0 and 9.0% w/v, respectively. GP blend at a concentration of 12.0% (w/v) in HFP showed good miscibility, resulting in a stable electrospinning process producing an electrospun scaffold showing a uniform structure at the macroscopic level. In order to increase the hydrophilicity and wettability of electrospun scaffolds,[58] CNCs were added as a filler to the GP blend in the amount of 1.0% (w/v). Surface wettability, crucial for tuning scaffold cell behavior, is strongly affected by the hydrophilic degree of the scaffold.[59]

Moreover, the El peptide (0.1% w/v) was employed as a filler in the NGP blend (CNCs/GE/PDLLA), not only for mimicking ECM composition with its presence but also for enabling cell incorporation.[32,33] The addition of CNCs and the El peptide afforded polymer solutions in HFP to final concentrations (w/v) of 13.0 and 13.1%, respectively.

XRD Analysis. Diffractograms of cellulose-containing uncross-linked NGP, ElNGP, and cross-linked NGP hybrid electrospun scaffolds were recorded and compared with the CNC powder as a reference. GP electrospun scaffolds were also investigated as negative control (Figure 1). The CNC powder diffractogram shows two peaks at $2\theta = 22.6$ and 34.6°, corresponding, respectively, to (2 0 0) and (0 0 4) reflections of crystallinity.[60] In the diffractograms of uncross-linked NGP and cross-linked NGP and ElNGP, a shoulder at $2\theta = 22.6°$ appeared as a contribution from the CNC component (black). Accordingly, the GP scaffold diffractogram that is devoid of CNCs, and therefore used as a negative control, did not show any shoulder or peak. Summarizing, XRD measurements demonstrated that CNCs retained their crystallinity when added as a coadjuvant in polymer mixtures. On that basis, we infer that the CNCs were successfully dispersed in polymer mixtures.

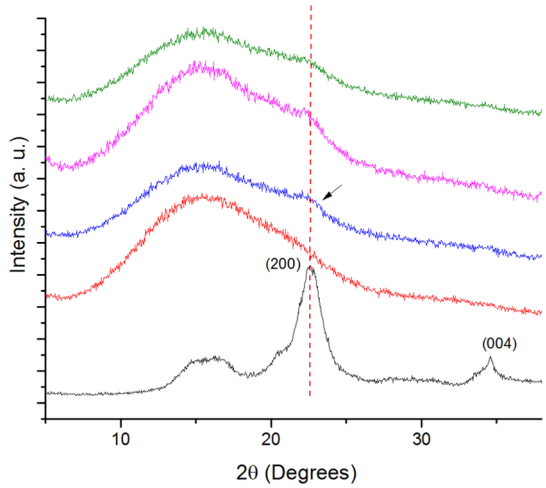

Figure 1. Diffractograms of electrospun scaffolds: CNC powder (black); GP (red); NGP (blue); ElNGP (magenta); and cross-linked NGP (green).

HPLC Analysis. The chromatograms obtained after treatment of the uncross-linked ElNGP scaffold in 85.5% ethanolic solution are shown in the Supporting Information and Figure S1. The uncross-linked ElNGP scaffold chromatogram (black curve in Figure S1a) shows the presence of a peak with a retention time (R_t) of 29.0 min that could be ascribed to the EX15 peptide by comparison with the chromatogram of the same peptide used as the reference (blue curve of Figure S1a in the Supporting Information). In contrast, the peak was not present in the chromatogram of the cross-linked ElNGP scaffold treated under the same conditions (data not shown). The rationale for the experimental findings could be that the EX15 peptide escaped from the scaffold into the reaction solution during the cross-linking reaction. In order to confirm the embedding of the EX15 peptide in the ElNGP scaffold during the cross-linking reaction, the uncross-linked ElNGP scaffold was treated in 45 mM EDC/NHS, as described before. The chromatogram (black curve of Figure S1b) did not show the peak assigned to the EX15 peptide under the cross-linking reaction conditions (R_t = 25.6 min) (blue curve in Figure S1b), proving on this basis that the EX15 peptide was fully embedded.

FT-IR Spectroscopy. FT-IR spectroscopy was used in order to analyze scaffolds at a molecular level. First, functional groups were assigned to pure polymers, and then they were used as a fingerprint for tracking the presence of a pure component in the hybrid scaffold spectra. From top to down, the first three FT-IR spectra in Figure 2 are ascribed to pure GE, CNCs, and PDLLA, while the remaining are related to GP, NGP, and ElNGP electrospun scaffolds. The FT-IR spectrum of GE showed at about 3521 cm^{-1} the amide A band (downward arrow), assigned to N−H stretching, and at approximately 3316 cm^{-1}, a broad band that originated from

https://dx.doi.org/10.1021/acsapm.0c00790
ACS Appl. Polym. Mater. 2020, 2, 4836−4847

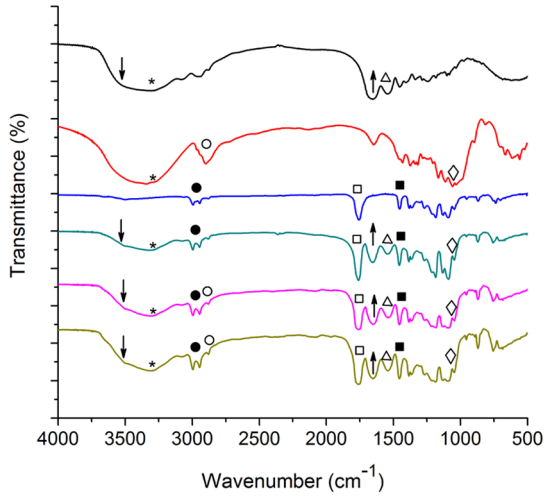

Figure 2. FT-IR spectra of GE (black); CNCs (red); PDLLA (blue); GP scaffold (dark cyan); NGP scaffold (magenta), and ElNGP scaffold (dark yellow).

O−H stretching (asterisk) of 4-hydroxyproline residues. At shorter wavenumbers, the amide I band at 1665 cm^{-1} (upward arrow) derived from peptide C═O stretching and the amide II band situated at 1551 cm^{-1} due to N−H bending (triangle), as hallmarks of proteins, were visible.[61]

Regarding the CNCs' FT-IR spectrum (red curve), a broad band can be noted from 3700 to 3100 cm^{-1} which is assigned to the stretching vibrations of carbohydrates' O−H groups (asterisk). Furthermore, bands due to aliphatic C−H stretching at about 2900 cm^{-1} (empty circle) and due to C−O stretching (diamond), typical of carbohydrates, were visible in the region ranging from 1200 to 1100 cm^{-1}.[53] The PDLLA FT-IR spectrum showed the aliphatic C−H stretching bands (filled circle) at 2995 and 2945 cm^{-1}, the ester C═O stretching (empty square) at 1760 cm^{-1}, and the C−H_3 bending (filled square) at 1454 cm^{-1}.[62] The FT-IR spectra of electrospun scaffolds are shown in Figure 2 as dark cyan, magenta, and dark yellow curves. Accordingly, the GP electrospun scaffold contains amide I (upward arrow), amide II (triangles), and A bands (downward arrow) from GE and aliphatic C−H (filled circle), C−H_3, (filled square), and ester C═O bands (empty square) from PDLLA.

In NGP electrospun scaffolds, the band due to O−H (asterisks) is also visible, together with aliphatic C−H stretching bands (filled and empty circles), derived from PDLLA and CNCs. In order to check if CNCs were successfully embedded in electrospun scaffolds, the bands' absorbance values from OH stretching and amide A were rated and the arithmetic ratio was calculated. The ratio values were equal to 1.1, 1.4, and 1.2 for GP, NGP, and ElNGP scaffolds, respectively. The data infer that in the NGP scaffold, a stronger contribution has been found from the stretching of the −OH groups. The smaller value found for ElNGP compared to NGP, even though CNCs are present in both scaffolds, is probably due to the contribution of additional N−H stretchings derived from the El peptide that is absent in NGP. The results demonstrate the successful incorporation of CNCs in the polymer mixture, confirming the efficiency of the electrospinning process.

Amine Group Content and Degree of Cross-Linking. The values of cross-linking degrees, calculated from the free amino group content after each treatment, indicated that the percentage of cross-linking of GP, NGP, and ElNGP is 91 ± 9, 100 ± 1, and 91 ± 1%, respectively. The results are expressed as mean values of three parallel measurements ± standard errors.

Cross-Linking Assessment. *ATR Spectroscopy.* In order to estimate the progression of the cross-linking reaction, we investigated GP electrospun scaffolds before and after the cross-linking reaction using ATR spectroscopy. In Figure 3,

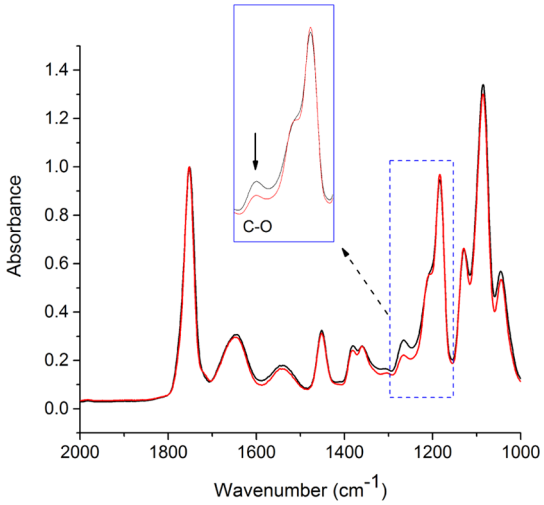

Figure 3. ATR spectra of GP electrospun scaffolds: before (black) and after cross-linking (red).

ATR spectra are shown in the region of interest comprised between 2000 and 1000 cm^{-1}. The presence of amide I and amide II bands from GE is evident in both samples. Our attention was focused on the bands at 1266 and 1541 cm^{-1}. The first band is assigned to the C−O stretching of carboxylic acid present in the side chains of Asp and Glu residues. The second band is attributed to N−H_2 bending from free ε-amine groups of lysine residues, both present in GE. In the spectrum of the cross-linked scaffolds of GP (red curve), the intensity of the band at 1266 cm^{-1} was considerably reduced and this feature was found in all three kinds of electrospun scaffolds: GP, NGP, and ElNGP (Figure S2). The intensity of the band at 1541 cm^{-1} was slightly lower too. These findings indicated the decrease in the number of carboxylic and free primary amine groups after the cross-linking reaction due to the formation of amide bonds according to the reaction scheme (Figure S3 in the Supporting Information).[63,64]

ATR spectra of uncross-linked and cross-linked GP electrospun scaffolds were slightly different, demonstrating that the reaction was successfully carried out.

SEM: Morphology, Fiber Diameter, and Porosity Evaluation. SEM was used to evaluate the electrospun scaffold morphology, as shown in Figure 4, with particular attention to the assessment of any defect (beads), investigating the fiber orientation and diameter distribution before and after the cross-linking reaction. The SEM image of the uncross-linked electrospun GP scaffold (Figure 4A) showed a well-defined three-dimensional fibrillar microstructure enriched with interconnected pores. It is worth noting that the interconnection was permanently visible even in the cross-linked sample (Figure 4D). The fibers appeared linear in the uncross-linked scaffold and curvilinear in the cross-linked one. In both cases, no traces of solvent and beads were detected, suggesting a

https://dx.doi.org/10.1021/acsapm.0c00790
ACS Appl. Polym. Mater. 2020, 2, 4836−4847

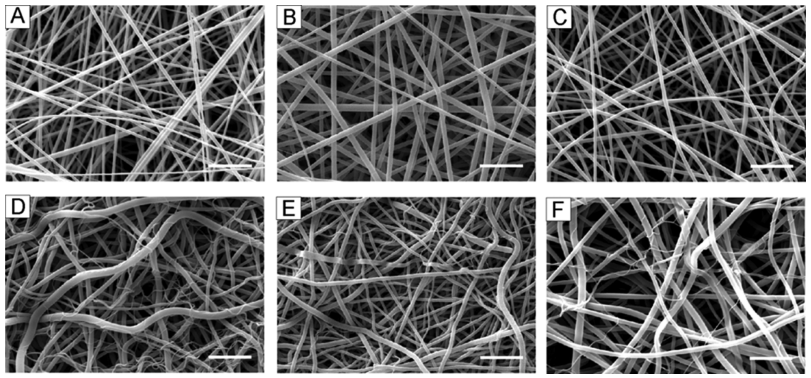

Figure 4. SEM images of electrospun scaffolds. Uncross-linked: GP (A), NGP (B), and ElNGP (C). Cross-linked: GP (D), NGP (E), and ElNGP (F); (bar: 10 μm).

good degree of dispersion of the polymers in the solvent.[65] Herein, EDC was used as a GE cross-linker[66−68] and is preferred to others, as vapor-phase glutaraldehyde could be potentially cytotoxic at certain concentrations,[69] and aqueous-phase genipin or glyceraldehyde gave rise to fused fibers. The average diameters of GP fibers as a frequency function are represented as a histogram (Figure S4A,B), showing a normal distribution around a mean value of 683 ± 174 nm and after the cross-linking reaction, the average diameter of the fibers increased from 683 ± 174 to 955 ± 240 nm (Table 2). The

Table 2. Scaffold Morphology

scaffold	average fiber diameter (nm)[a]	wettability (%)	porosity (%)
GP	683 ± 174	n. d.	68 ± 2
GP cross-linked	955 ± 240	374 ± 28	59.5 ± 0.6
NGP	1116 ± 290	n. d.	66.1 ± 0.7
NGP cross-linked	828 ± 280	449 ± 26	62 ± 1
ElNGP	823 ± 216	n. d.	63 ± 1
ElNGP cross-linked	1176 ± 344	607 ± 52	51 ± 3

[a]Mean value ± standard deviation (n > 1000 from three different images).

SEM image of the uncross-linked NGP scaffold (Figure 4B) showed fibrillar and interconnected porous microstructures presenting randomly oriented fibers forming a nonwoven matrix with a normal distribution around a mean value of 1116 ± 290 nm (Figure S4C,D). The striking analogy with the uncross-linked GP electrospun scaffold is an indirect inspection of the homogeneousness of dispersion and the efficiency of the electrospinning process, despite the presence of CNCs. Interestingly, unpromising results were obtained from cellulose microcrystals (CMCs) when added to a polymer blend. Indeed, in related SEM images, the presence of CMCs induced the excessive enlargement of the fibers probably due to the scale dimension of CMCs, micro—instead of nano—, as reported by Jia et al.[70] After the cross-linking reaction, the NGP scaffold presented a change in the orientation of the fibers assuming a curvilinear shape (Figure 4E). Diverse to previous results, the cross-linking reaction performed on the CNC hybrid scaffold induced the decrease of the average diameter of the fibers from 1116 ± 290 to 828 ± 290 nm (Table 2).

Concerning the ElNGP electrospun hybrid scaffold obtained after the addition of the EX15 peptide, neither the fibrillar nor the interconnected porous microstructures were affected (Figure 4C).[66,71] Analogous to GP, the cross-linking reaction triggered the curling of fibers (Figure 4F) with the average diameter growing from 823 ± 216 to 1176 ± 344 nm (Figure S4E,F). To evaluate if the average diameter values found were statistically different from each other, statistical analyses were performed using the one-way ANOVA method and Tukey's test (Figure S5). The results showed that the average diameters of the fibers of uncross-linked scaffolds are statistically different from those of cross-linked samples. The different morphology of cross-linked fibers, different in orientation and size, is an indirect proof of the accomplishment of the cross-linking reaction.

The persistence of porous interconnected structures could make these scaffolds appealing as biomedical devices able to assure oxygen and vapor permeation. Furthermore, the fibrillar organization mimics the natural ECM matrix hierarchically organized in fibrillar structures of different sizes from El, collagen, and polysaccharides. These features could make the produced scaffolds appealing for wound dressing. As a matter of fact, wound dressings are required to absorb exudates and at the same time to ensure oxygen permeation.

MacLellan and co-workers reported that scaffolds presenting ∼880 nm fiber diameter might be optimal for soft tissue engineering applications,[72] even if the assessment of the best fibril size is difficult to claim from the perspective of the wide pool of potential polymers to use, while antibacterial dressings with fiber diameters ranging from 0.2 to 3 μm showed healing efficacy.[73]

Furthermore, the addition of CNCs to GP led to a significant increase of the average diameter of the fibers, with $p^* \leq 0.01$ (from 683 ± 174 to 1116 ± 290 nm, Table 2). This finding is probably due to an increase in the polymer solution viscosity,[74] in agreement with literature data on electrospun blends made of PLGA[75] at different percentages of CNCs; however, CNCs have also been suggested to induce the opposite effect on the fiber diameter through their reduction.[76,77] This behavior could be explained by an increase of electric conductivity of the polymer solutions. As a matter of fact, CNCs are usually produced through acid hydrolysis of cellulose, generally through H_2SO_4,[38] leaving sulfate groups on them, causing an increase of the electrical charge and, consequently, the electrical conductivity of the electrospun solution and a decrease in the average diameter of the fibers. These two different effects act in opposition to each other: in the case of NGP, the increase in the polymer solution viscosity

https://dx.doi.org/10.1021/acsapm.0c00790
ACS Appl. Polym. Mater. 2020, 2, 4836−4847

prevailed on enhanced electrical conductivity. On the contrary, the addition of EX-15 peptide led to a significant decrease of the average diameter of fibers according to Swindle-Reilly et al.,[78] who reported electrospun scaffolds composed of a PCL/El blend in HFP having a diameter of fibers that is significantly smaller than that of neat PCL ones, due to peptide incorporation into the fiber network.

Commonly, porosity is important to dictate cellular infiltration and tissue ingrowth into the scaffolds.[79] Looking at literature, one can observe that Ameer et al. have presented many strategies to tune electrospun scaffold porosity to enhance the cell response in tissue engineering.[80] The porosity of scaffolds studied in this work has been evaluated, with the results summarized in Table 2 and statistical analysis in Figure S6.

Uncross-linked and cross-linked scaffolds showed similar porosity: GP, NGP, and ElNGP displayed calculated values of 68 ± 2, 66.1 ± 0.7, and 63 ± 1%, respectively, with a decrease for their cross-linked scaffolds (59.5 ± 0.6, 62 ± 1, and 51 ± 3% for GP, NGP, and ElNGP, respectively). Statistical analysis showed that the decrease was significant only for GP and ElNGP scaffolds, and that the cross-linking reaction induced a slight decrease of porosity in all electrospun scaffolds.

Cross-linking of the scaffolds by the EDC/NHS protocol performed in ethanol/water solution determined a variation in fiber diameters and porosity due to a macroscopically evident shrinkage. Figure 5 exhibits a scaffold showing a shrinkage of

Figure 5. Shrinkage of the electrospun scaffold after the cross-linking reaction (NHS and EDC·HCl = 45.0 mM in 85.5% ethanolic solution, RT, overnight).

the diameter from 9 to 4.5 cm after cross-linking. Other authors observed similar findings, which are particularly evident in scaffolds containing a high content of GE.[55,81]

GE gels studied at ethanol concentrations >40% v/v exhibited a volume shrinkage that can be extended to values of 25−50%.[82] Plausibly, the cross-linking reaction performed at a high ethanol concentration (85%, v/v) determined a shrinking effect on GE, ascribed to deswelling. In the case of microfiber shrinkage, a decrease in the fiber length translated into an increase in the fiber diameter,[83] a reduction of porosity, and a higher density of the scaffold.

Swelling Test and Contact Angle Measurements. The swelling test was carried out on the cross-linked scaffolds to evaluate their capacity to absorb water, thereby indirectly testing their hydrophobicity degree. The average swelling of the scaffolds, expressed in terms of percentages and calculated according to eq 1, afforded values of 374 ± 28, 449 ± 26, and 607 ± 52% for GP, NGP, and ElNGP scaffolds, respectively (Table 2), thus demonstrating the progressive increase of wettability with CNC and El contents. Statistical analysis was performed on these values using Student's *t*-test (Figure S7), displaying a statistical difference ($*p \leq 0.01$).

Even if it is in a speculative way, the rationale for the observed increase of wettability with CNCs and EX15 is the onset of hydrogen bonding network between water, cellulose hydroxyl moieties, and peptide polyamide groups. Nevertheless, all electrospun scaffolds showed strong hydrophilicity due to their swift water drop absorption (less than 2 s), during contact angle measurements. That finding is worth noting if we consider that PDLLA, similar to PLA, is usually considered highly hydrophobic. Therefore, we successfully modified the physical characteristics of hybrid electrospun scaffolds by mixing polymers having complementary properties: the highly hydrophilic polymers GE, CNCs, and El mitigated the hydrophobicity of PLA. In summary, even if with some differences, all scaffolds showed total wettability, suggesting their employment as a wound dressing material, as a low degree of hydrophobicity is the best for biomedical devices. Highly hydrophilic wound dressing, indeed, prevents scab formation and dehydration of the wound bed.[84]

Uniaxial Tensile Testing. In order to evaluate the mechanical properties, uniaxial tensile testing on cross-linked GP, NGP, and ElNGP scaffolds was conducted. Young's modulus and ultimate tensile strength calculations were carried out on dry and swollen scaffolds (Table 3). Young's moduli

Table 3. Mechanical Properties[a]

scaffold	Young's modulus (MPa)	ultimate tensile strength (MPa)	elongation at break (%)
GP	87 ± 13	6.5 ± 0.6	57.2 ± 32.6
GP after swelling	24 ± 4	4.0 ± 0.3	>120
NGP	75 ± 14	6.2 ± 0.4	104.0 ± 18.1
NGP after swelling	27 ± 3	4.1 ± 0.3	>120
ElNGP	75 ± 15	6.3 ± 0.3	113.8 ± 8.3
ElNGP after swelling	23 ± 4	4.0 ± 0.2	>120

[a]Values of the Young's modulus and ultimate tensile strength calculated for the electrospun scaffolds before and after the swelling test.

were 87 ± 13, 75 ± 14, and 75 ± 15 MPa for dry GP, NGP, and ElNGP, respectively. Moreover, statistical analysis (Figure S8A) evidenced that for NGP and ElNGP, Young's modulus is significantly different from GP ($p* \leq 0.05$), inferring an influence of CNCs. As recently reported,[85,86] the addition of small percentages of CNCs to PLA (5% based on the weight) led to an increase of the Young's modulus and tensile properties as well. Conversely, for values higher than 5%, a decrease in the Young's modulus has been observed, probably because of the self-aggregation of CNCs in electrospun fibers being responsible for the weakening of the cohesion among them.[85] It is well known that the source of CNCs and their production should be taken into account, as they affect the rheology of the electrospun solution and then the mechanical properties of the final fibers. In the present study, commercial CNCs employed presented a low aspect ratio, with shear-thinning behavior. The increase of the viscosity in comparison with neat PLA, as reported by Hamad and co-workers,[87] generally affects the fiber diameter of electrospun scaffolds. It, in turn, influences the mechanical properties.

https://dx.doi.org/10.1021/acsapm.0c00790
ACS Appl. Polym. Mater. 2020, 2, 4836−4847

CNCs were added at a final concentration of 8.3% (w/w) in the NGP scaffold and 8.2% (w/w) in the ElNGP scaffold expressed on the total mass of the remaining components in polymer solutions inducing the decrease of Young's modulus. That finding is important because we suggested that it is possible to modify the scaffold elasticity and optimize the mechanical properties of PLA-based scaffolds.

After swelling the scaffolds in water, a dramatic change in the Young's modulus value was observed, affording 24 ± 4, 27 ± 3, and 23 ± 4 MPa for GP, NGP, and ElNGP scaffolds, respectively. The values observed by comparing the dry state with the swollen ones were significantly different ($p^* \leq 0.05$) (Figure S8B,C), and swollen scaffolds appear more elastic.

Young's modulus values are compatible with those found for scaffolds with applications in soft tissue engineering, such as, for example, of natural skin showing a tensile modulus of 15−150 MPa compatible with our scaffolds having Young's modulus within this range.[88] Uniaxial tensile testing (UTS values) in the dry state were 6.5 ± 0.6, 6.2 ± 0.4, and 6.3 ± 0.3 MPa for GP, NGP, and ElNGP scaffolds, respectively. The corresponding swollen scaffolds showed UTS values of 4.0 ± 0.3, 4.1 ± 0.3, and 4.0 ± 0.2 MPa, respectively. However, also in that case, changes were not significant ($p > 0.05$) (Figure S9A,B). On the contrary and analogous to Young's modulus, UTS values of dry scaffolds significantly differ from swollen samples ($p^* \leq 0.05$) (Figure S9C). It is interesting to note that NGP and ElNGP scaffolds show the greatest elongation at break in the dry state [elongation (%) = 57.2 ± 32.6, 104 ± 18.1, and 113.8 ± 8.3% for GP, NGP, and ElNGP, respectively], as shown in Table 3 and Figures S10C,E.

Studies of MacLellan and co-workers, in the production of electrospun PCL-composite scaffolds for soft tissue engineering,[72] reported that electrospun GE scaffolds presented, in the dry state, correspondingly higher tensile strength and lower brittleness than the collagen and El ones. Our scaffolds in the dry state, as well, showed UTS values along the same lines varying from ∼6 to ∼4 MPa after swelling.

Plasticizers can increase the free volume between the polymer chains leading to greater chain mobility and film flexibility. Generally, El exerts its elastic function in a solid—although in a swollen state—when immersed in water. The aqueous solvent interacts with the amorphous regions of the protein. Actually, water and polar solvents such as dimethylsulfoxide exert a plasticizer effect on El, that is, they facilitate the localized movements of the polypeptide chains.[89] In our case, the polar solvent destructures the β-sheet of EX15.[33] The consequence is the increase of the entropy of the system and the onset of the entropic elastomeric force.

The addition of a plasticizer would increase the elongation. NGP and ElNGP, indeed, exhibit higher elongation at rupture than that of the GP hybrid scaffold in the dry state (Figure S10C−E). Moreover, a plasticized polymer would be less resilient and would deform at a lower force than without the plasticizer. The Young's modulus is the slope of the linear section on the stress−strain curve where a polymer undergoes elastic deformation, and because there is greater chain mobility with the addition of a plasticizer, there is less resistance to deformation, hence a lower Young's modulus is expected.[90]

These considerations explain why CNC and El hybrid scaffolds are less brittle in the swollen state. Nevertheless, our data are in good agreement with data inferred for microfibrillated cellulose incorporating materials acting as a plasticizer.[91] Water instead acts as a sort of normalizer for the different typologies of scaffolds because all swollen electrospun scaffolds reach a plateau with an elongation (%) > 100% at break (Figure S10). This behavior is in accordance with previous data.[55]

Cytotoxicity Assay. The results of the cytotoxicity assay showed no negative influence of the polymer extracts on the metabolic activity of NIH/3T3 cells (Figure 6). The cells in the extraction medium of GP and NGP showed an even higher metabolic activity (117 and 104%, respectively) than the negative control. However, the difference was not significant. Only the metabolic activity of cells in the ElNGP-extracted medium was slightly lower than that in the negative control (87%). According to ISO 10993-5:2009, the extract shows no cytotoxic potential if the relative viability is not reduced below 70%. This condition was met in this cytotoxicity test for all three polymers. The scaffolds were spun out of polymers, which were previously described as mostly biocompatible. Even if PLA, which is approved by the FDA for use in medical devices, is highly biocompatible,[92] to the best of our knowledge, only data regarding the cytotoxicity of poly(D/L-lactide-co-L-lactide) have been reported;[93] that finding required a cytotoxic assay on PDLLA, which shows faster degradation than the semicrystalline PLA. In combination with GE, no cytotoxic effects on human skin fibroblasts were observed.[55]

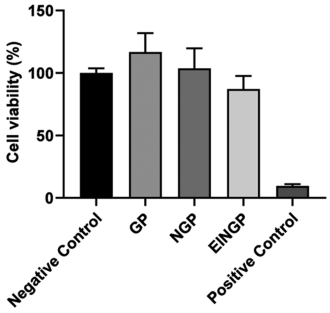

Figure 6. Cytotoxic assay of different cross-linked electrospun microfibers on the metabolic activity of NIH/3T3 cells.

The influence of CNCs on cells is described rather controversially. No cytotoxicity on fibroblast cells was observed for CNCs with PLGA,[94] PLA, and PBS matrices.[95] Nanofibers based on PLA and CNCs proved to be biocompatible.[96,97] However, the cytotoxic effect at high-CNC concentrations was described as well.[98] Electrospun El in combination with silk[99] and collagen[50] showed the absence of cytotoxicity.

Cell Attachment and Proliferation. The cell culture on different scaffold types showed the attachment and proliferation of L929 cells for different time points (Figure 7). It turns out that the cells adhered to and spread on the surface of all scaffold types from day 1 to day 5. There was a significant increase in cell densities for all scaffold types over the entire culture period (Figure 7a, Table S1). Whereas at day 1, only few cells were observed on the scaffold surface, at day 5, the cells reached confluence on all scaffold types. It should be noted that the cells do not detach, even at a high cell density. Besides, it shows no significant different number of adherent cells between the scaffold types except on day 5 NGP versus ElNGP (1986 ± 415 cells/mm^2 vs 2312 ± 290 mm^2, $p < 0.05$). The F-actin staining of L929 showed a stretched morphology of the cells at day 1 and day 3, whereas the cells at day 5 form a

https://dx.doi.org/10.1021/acsapm.0c00790
ACS Appl. Polym. Mater. 2020, 2, 4836−4847

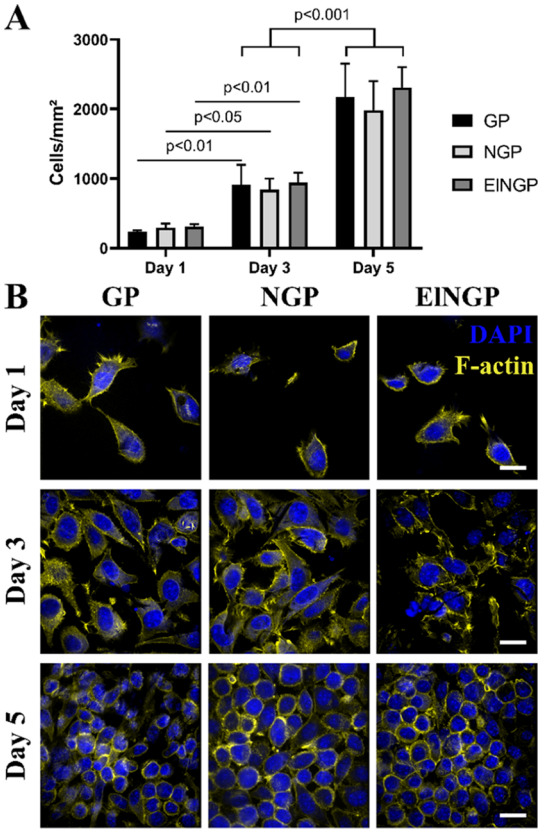

Figure 7. Attachment and proliferation of L929 cells on different scaffold types GP, NGP, and ElNGP. (A) Quantification of attached L929 cells after 1, 3, and 5 days. Two-way ANOVA, n = 3. (B) Nucleus and F-actin staining of L929 cells. Scale bar equals 20 μm.

roundish morphology (Figure 7b). The change in the cell morphology corresponds to the behavior of L929 cells, as shown by Hong et al.[100] and Koegler et al.[101]

In conclusion, this work confirmed the findings from previous studies, which showed that electrospun scaffolds made of materials such as GE, El, and CNCs have good biocompatibility in terms of cell attachment and proliferation.[50,55,102]

CONCLUSIONS

In this work, we produced electrospun scaffolds made of green and nature-inspired polymers. GE, PDLLA, CNCs, and El were carefully chosen as scaffold components because of their complementary properties in terms of hydrophobicity, bioactivity, elasticity, and bioresorbability. The achievement of processing parameters by electrospinning let the production of scaffolds with uniform morphology at a macroscopic level and devoid of any defects or beads at a microscopic level. FT-IR spectra in the solid state characterized scaffolds at the molecular level. The successful embedding in the scaffolds of crystalline CNCs and of El as well was assessed by XRD and HPLC analysis, respectively. Electrospun scaffolds were cross-linked for the presence of GE and the quantitative degree of cross-linking was evaluated by the TNBS assay. Further insights into the success of the cross-linking reaction were obtained by ATR spectroscopy revealing molecular changes triggered by the cross-linking reaction. One of the main challenges inherent to 3D reticulation of scaffolds is represented by the occlusion of pores. Herein, we demonstrated that EDC and NHS did not seal the network of interconnected pores, as revealed by SEM. We have characterized the electrospun scaffolds through the investigation of the dimensions of the electrospun fibers, their wettability, elasticity, and resistance to rupture as well. For the first time, we have combined El and nanocellulose in GP electrospun scaffolds. The results were encouraging and the electrospun scaffolds showed good potential. As a future perspective, we will tune the route and conditions paying particular attention to El and nanocellulose concentrations. The present study suggests, in the first instance, that CNCs could be used not only as reinforcement but also as a plasticizer for improving the levels of compliance before failure of the material. Additionally, we demonstrated that brittleness decreases in the swollen state. Last but not least, non-cytotoxicity, cell attachment, and proliferation were evaluated for all electrospun scaffolds. Finally, we suggest wound dressing applications as potential use for CNC- and El-containing electrospun membranes. As a matter of fact, the improved mechanical properties observed in the dry state are crucial for the comfortable application of the dressing on the wound. The presence of CNCs and El on the one hand would reduce brittleness and on the other would improve water uptake, which is considered an essential feature in wound dressing applications.[103] Studies on this aspect are underway.

ASSOCIATED CONTENT

Supporting Information

The Supporting Information is available free of charge at https://pubs.acs.org/doi/10.1021/acsapm.0c00790.

Cross-linking reaction of GE, fiber diameter analysis, HPLC chromatograms, average swelling test (%), Young's modulus, and UTS (PDF)

AUTHOR INFORMATION

Corresponding Author

Brigida Bochicchio − *Laboratory of Protein Chemistry, Laboratory of Bioinspired Materials (LaBIM), Department of Science, University of Basilicata, 85100 Potenza, Italy;* orcid.org/0000-0002-0700-9257; Phone: +39 0971 20 54 81; Email: brigida.bochicchio@unibas.it

Authors

Nicola Ciarfaglia − *Laboratory of Protein Chemistry, Laboratory of Bioinspired Materials (LaBIM), Department of Science, University of Basilicata, 85100 Potenza, Italy*

Antonietta Pepe − *Laboratory of Protein Chemistry, Laboratory of Bioinspired Materials (LaBIM), Department of Science, University of Basilicata, 85100 Potenza, Italy;* orcid.org/0000-0002-1285-2273

Germano Piccirillo − *Laboratory of Protein Chemistry, Laboratory of Bioinspired Materials (LaBIM), Department of Science, University of Basilicata, 85100 Potenza, Italy; Department of Women's Health, Research Institute for Women's Health, Eberhard-Karls-University Tübingen, 72076 Tübingen, Germany*

Antonio Laezza − *Laboratory of Protein Chemistry, Laboratory of Bioinspired Materials (LaBIM), Department of Science, University of Basilicata, 85100 Potenza, Italy*

Ruben Daum − *NMI Natural and Medical Sciences Institute at the University of Tübingen, 72770 Reutlingen, Germany*

https://dx.doi.org/10.1021/acsapm.0c00790
ACS Appl. Polym. Mater. 2020, 2, 4836−4847

Katja Schenke-Layland − *NMI Natural and Medical Sciences Institute at the University of Tübingen, 72770 Reutlingen, Germany; Department of Women's Health, Research Institute for Women's Health, Eberhard-Karls-University Tübingen, 72076 Tübingen, Germany; Cluster of Excellence iFIT (EXC 2180) "Image-Guided and Functionally Instructed Tumor Therapies", University of Tübingen, 72076 Tübingen, Germany; Department of Medicine/Cardiology, Cardiovascular Research Laboratories, David Geffen School of Medicine at UCLA, Los Angeles, California 90095, United States*

Complete contact information is available at: https://pubs.acs.org/10.1021/acsapm.0c00790

Author Contributions

The manuscript was written through contributions of all authors.

Notes

The authors declare no competing financial interest.

■ ACKNOWLEDGMENTS

The authors thank Alessandro Laurita (Microscopy Center, University of Basilicata, Potenza, Italy) for SEM images. Special thanks are due to Jany Dandurand (Université Toulouse III, Toulouse, France) for ATR spectroscopy. The authors are grateful for the financial support by PON R&I 2014-2020 (cod: PON_ARS01_01081 and PON_AIM1852803 Linea 1) from MIUR.

■ REFERENCES

(1) Miao, Y.-E.; Liu, T. Electrospun Nanofiber Electrodes: A Promising Platform for Supercapacitor Applications. In *Electrospinning: Nanofabrication and Applications*; Ding, B., Wang, X., Yu, J., Eds.; Elsevier: Amsterdam, Netherlands, 2019; pp 641−669.

(2) Lu, P.; Murray, S.; Zhu, M. Electrospun Nanofibers for Catalysts. In *Electrospinning: Nanofabrication and Applications*; Ding, B., Wang, X., Yu, J., Eds.; Elsevier: Amsterdam, Netherlands, 2019; pp 695−717.

(3) Sankar, S. S.; Ede, S. R.; Anantharaj, S.; Karthick, K.; Sangeetha, K.; Kundu, S. Electrospun cobalt-ZIF micro-fibers for efficient water oxidation under unique pH conditions. *Catal. Sci.* **2019**, *9*, 1847−1856.

(4) Sun, Y.; Cheng, S.; Lu, W.; Wang, Y.; Zhang, P.; Yao, Q. Electrospun fibers and their application in drug con-trolled release, biological dressings, tissue repair, and enzyme immobilization. *RSC Adv.* **2019**, *9*, 25712−25729.

(5) Xue, J.; Niu, Y.; Gong, M.; Shi, R.; Chen, D.; Zhang, L.; Lvov, Y. Electrospun microfiber membranes embedded with drug-loaded clay nanotubes for sustained antim-icrobial protection. *ACS Nano* **2015**, *9*, 1600−1612.

(6) Cui, W.; Zhou, Y.; Chang, J. Electrospun nanofibrous ma-terials for tissue engineering and drug delivery. *Sci. Technol. Adv. Mater.* **2010**, *11*, 014108.

(7) Agarwal, S.; Wendorff, J. H.; Greiner, A. Progress in the Field of Electrospinning for Tissue Engineering Applications. *Adv. Mater.* **2009**, *21*, 3343−3351.

(8) Patel, K. D.; Kim, H. W.; Knowles, J. C.; Poma, A. Molecularly imprinted polymers and electrospinning: manufacturing convergence for next-level Applications. *Adv. Funct. Mater.* **2020**, *30*, 2001955−2001970.

(9) Chen, W.; Tian, X.; He, W.; Li, J.; Feng, Y.; Pan, G. Emerging functional materials based on chemically designed molecular recognition. *BMC Mater.* **2020**, *2*, 1.

(10) Jenkins, T. L.; Little, D. Synthetic scaffolds for musculoskeletal tissue engineering: cellular responses to fiber parameters. *npj Regener. Med.* **2019**, *4*, 15−28.

(11) Hinderer, S.; Layland, S. L.; Schenke-Layland, K. ECM and ECM-like materials - Biomaterials for applications in regenerative medicine and cancer therapy. *Adv. Drug Delivery Rev.* **2016**, *97*, 260−269.

(12) Sandri, G.; Rossi, S.; Bonferoni, M. C.; Caramella, C.; Ferrari, F. Electrospinning Technologies in Wound Dressing Applications. In *Therapeutic Dressings and Wound Healing Applications*; Boateng, J., Ed.; John Wiley & Sons, Inc.: Hoboken, NJ, 2020; pp 315−336.

(13) Nyilas, E.; Chiu, T. H. Bioresorbable Polyesters and Polyester Composites. U.S. Patent 4,481,353 A, October 7, 1983.

(14) Gao, X.; Han, S.; Zhang, R.; Liu, G.; Wu, J. Progress in electrospun composite nanofibers: composition, performance and applications for tissue engineering. *J. Mater. Chem. B* **2019**, *7*, 7075−7089.

(15) Singhvi, M. S.; Zinjarde, S. S.; Gokhale, D. V. Polylactic acid: synthesis and biomedical applications. *J. Appl. Microbiol.* **2019**, *127*, 1612−1626.

(16) Gupta, B.; Revagade, N.; Hilborn, J. Poly(lactic acid) fiber: An overview. *Prog. Polym. Sci.* **2007**, *32*, 455−482.

(17) Fambri, L.; Pegoretti, A.; Fenner, R.; Incardona, S. D.; Migliaresi, C. Biodegradable fibres of poly(l-lactic acid) produced by melt spinning. *Polymers* **1997**, *38*, 79−85.

(18) Reddy, G.; Altaf, M.; Naveena, B. J.; Venkateshwar, M.; Kumar, E. V. Amylolytic bacterial lactic acid fermentation - a review. *Biotechnol. Adv.* **2008**, *26*, 22−34.

(19) Fukushima, K.; Sogo, K.; Miura, S.; Kimura, Y. Production of D-Lactic Acid by Bacterial Fermentation of Rice Starch. *Macromol. Biosci.* **2004**, *4*, 1021−1027.

(20) Dorgan, J. R.; Lehermeier, H.; Mang, M. Thermal and Rheological Properties of Commercial-Grade Poly(Lactic Acid)s. *J. Polym. Environ.* **2000**, *8*, 1−9.

(21) Desguin, B.; Soumillion, P.; Hausinger, R. P.; Hols, P. Unexpected complexity in the lactate racemization sys-tem of lactic acid bacteria. *FEMS Microbiol. Rev.* **2017**, *41*, S71−S83.

(22) Salminen, S.; Wright, A. V.; Ouwehand, A. *Lactic Acid Bacteria: Microbiological and Functional Aspects*, 3rd ed., Revised and Expanded; Marcel Dekker, Inc.: New York, NY, 2004.

(23) Goffin, P.; Deghorain, M.; Mainardi, J.-L.; Tytgat, I.; Champomier-Vergés, M.-C.; Kleerebezem, M.; Hols, P. Lactate racemization as a rescue pathway for supplying D-lactate to the cell wall biosynthesis machinery in Lactobacillus plantarum. *J. Bacteriol.* **2005**, *187*, 6750−6761.

(24) Stetter, K. O.; Kandler, O. Formation of DL-lactic acid by lactobacilli and characterization of a lactic acid ra-cemase from several streptobacteria. *Arch. Mikrobiol.* **1973**, *94*, 221−247.

(25) Hiyama, T.; Fukui, S.; Kitahara, K. Purification and properties of lactate racemase from Lactobacillus sake. *J. Biochem.* **1968**, *64*, 99−107.

(26) Casalini, T.; Rossi, F.; Castrovinci, A.; Perale, G. A perspective on polylactic acid-based polymers use for nanoparticle synthesis and applications. *Front. Bioeng. Biotechnol.* **2019**, *7*, 259−274.

(27) Madhavan Nampoothiri, K.; Nair, N. R.; John, R. P. An overview of the recent developments in polylactide (PLA) research. *Bioresour. Technol.* **2010**, *101*, 8493−8501.

(28) Inkinen, S.; Hakkarainen, M.; Albertsson, A.-C.; Södergård, A. From lactic acid to poly(lactic acid) (PLA): characterization and analysis of PLA and its precursors. *Biomacromolecules* **2011**, *12*, 523−532.

(29) Bochicchio, B.; Barbaro, K.; De Bonis, A.; Rau, J. V.; Pepe, A. Electrospun poly(d,l-lactide)/gelatin/glass-ceramics tricomponent nanofibrous scaffold for bone tissue engineering. *J. Biomed. Mater. Res., Part A* **2020**, *108*, 1064−1076.

(30) Alippilakkotte, S.; Sreejith, L. Benign route for the modification and characterization of poly(lactic acid) (PLA) scaffolds for medicinal application. *J. Appl. Polym. Sci.* **2018**, *135*, 46056−46068.

(31) Eskandarinia, A.; Kefayat, A.; Agheb, M.; Rafienia, M.; Baghbadorani, M. A.; Navid, S.; Ebrahimpour, K.; Khodabakhshi, D.; Ghahremani, F. A Novel Bilayer Wound Dressing Composed of a Dense Polyurethane/Propolis Membrane and a Biodegradable

Polycaprolactone/Gelatin Nanofibrous Scaffold. *Sci. Rep.* **2020**, *10*, 3063−3077.
(32) Yeo, G. C.; Aghaei-Ghareh-Bolagh, B.; Brackenreg, E. P.; Hiob, M. A.; Lee, P.; Weiss, A. S. Fabricated Elastin. *Adv. Healthcare Mater.* **2015**, *4*, 2530−2556.
(33) Tamburro, A. M.; Pepe, A.; Bochicchio, B. Localizing α-Helices in Human Tropoelastin: Assembly of the Elastin "Puzzle". *Biochemistry* **2006**, *45*, 9518−9530.
(34) Natarajan, S.; Harini, K.; Gajula, G. P.; Sarmento, B.; Neves-Petersen, M. T.; Thiagarajan, V. Multifunctional magnetic iron oxide nanoparticles: diverse synthetic approaches, surface modifications, cytotoxicity towards biomedical and industrial applications. *BMC Mater.* **2019**, *1*, 2.
(35) Liu, C.; Xu, X.; Zhou, J.; Yan, J.; Wang, D.; Zhang, H. Redox-responsive tumor targeted dual-drug loaded biocompatible metal−organic frameworks nanoparticles for enhancing anticancer effects. *BMC Mater.* **2020**, *2*, 7.
(36) Liu, S.; Qin, S.; He, M.; Zhou, D.; Qin, Q.; Wang, H. Current applications of poly(lactic acid) composites in tissue engineering and drug delivery. *Composites, Part B* **2020**, *199*, 108238−108262.
(37) Hashaikeh, R.; Krishnamachari, P.; Samad, Y. A. Nano-manifestation of Cellulose: Applications for Bio-degradable Composites. In *Handbook of Polymer Nanocomposites Processing, Performance and Application: Volume C: Polymer Nanocomposites of Cellulose Nanoparticles*; Pandey, J. K., Takagi, H., Nakagaito, A. N., Kim, H.-J., Eds.; Springer: New York, NY, 2015; pp 229−248.
(38) Habibi, Y.; Lucia, L. A.; Rojas, O. J. Cellulose nanocrystals: chemistry, self-assembly, and applications. *Chem. Rev.* **2010**, *110*, 3479−3500.
(39) Beck-Candanedo, S.; Roman, M.; Gray, D. G. Effect of Reaction Conditions on the Properties and Behavior of Wood Cellulose Nanocrystal Suspensions. *Biomacromolecules* **2005**, *6*, 1048−1054.
(40) Sakurada, I.; Nukushina, Y.; Ito, T. Experimental determination of the elastic modulus of crystalline regions in oriented polymers. *J. Polym. Sci.* **1962**, *57*, 651−660.
(41) Yu, H.-Y.; Wang, C.; Abdalkarim, S. Y. H. Cellulose nanocrystals/polyethylene glycol as bifunctional rein-forcing/compatibilizing agents in poly(lactic acid) nano-fibers for controlling long-term in vitro drug release. *Cellulose* **2017**, *24*, 4461−4477.
(42) Ben Shalom, T.; Nevo, Y.; Leibler, D.; Shtein, Z.; Azerraf, C.; Lapidot, S.; Shoseyov, O. Cellulose Nanocrystals (CNCs) Induced Crystallization of Polyvinyl Alcohol (PVA) Super Performing Nanocomposite Films. *Macromol. Biosci.* **2019**, *19*, 1800347.
(43) Fan, Z.; Liu, B.; Wang, J.; Zhang, S.; Lin, Q.; Gong, P.; Ma, L.; Yang, S. A Novel Wound Dressing Based on Ag/Graphene Polymer Hydrogel: Effectively Kill Bacteria and Accelerate Wound Healing. *Adv. Funct. Mater.* **2014**, *24*, 3933−3943.
(44) Davidenko, N.; Campbell, J. J.; Thian, E. S.; Watson, C. J.; Cameron, R. E. Collagen-hyaluronic acid scaffolds for adipose tissue engineering. *Acta Biomater.* **2010**, *6*, 3957−3968.
(45) Ofner, C. M., III; Bubnis, W. A. Chemical and swelling evaluations of amino group cross-linking in gelatin and modified gelatin matrices. *Pharm. Res.* **1996**, *13*, 1821−1827.
(46) Schindelin, J.; Arganda-Carreras, I.; Frise, E.; Kaynig, V.; Longair, M.; Pietzsch, T.; Preibisch, S.; Rueden, C.; Saalfeld, S.; Schmid, B.; Tinevez, J.-Y.; White, D. J.; Hartenstein, V.; Eliceiri, K.; Tomancak, P.; Cardona, A. Fiji: an open-source platform for biological-image analysis. *Nat. Methods* **2012**, *9*, 676−682.
(47) Annis, D.; Bornat, A.; Edwards, R. O.; Higham, A.; Loveday, B.; Wilson, J. An elastomeric vascular pros-thesis. *Trans.—Am. Soc. Artif. Intern. Organs* **1978**, *24*, 209−214.
(48) Li, M.; Mondrinos, M. J.; Chen, X.; Gandhi, M. R.; Ko, F. K.; Lelkes, P. I. Co-electrospun poly(lactide-co-glycolide), gelatin, and elastin blends for tissue engineering scaffolds. *J. Biomed. Mater. Res., Part A* **2006**, *79*, 963−973.
(49) Kumbar, S. G.; Nukavarapu, S. P.; James, R.; Nair, L. S.; Laurencin, C. T. Electrospun poly(lactic acid-co-glycolic acid) scaffolds for skin tissue engineering. *Biomaterials* **2008**, *29*, 4100−4107.
(50) Rnjak-Kovacina, J.; Wise, S. G.; Li, Z.; Maitz, P. K. M.; Young, C. J.; Wang, Y.; Weiss, A. S. Electrospun synthetic human elastin:collagen composite scaffolds for dermal tissue engineering. *Acta Biomater.* **2012**, *8*, 3714−3722.
(51) Lalia, B. S.; Guillen, E.; Arafat, H. A.; Hashaikeh, R. Nanocrystalline cellulose reinforced PVDF-HFP membranes for membrane distillation application. *Desalination* **2014**, *332*, 134−141.
(52) Zoppe, J. O.; Peresin, M. S.; Habibi, Y.; Venditti, R. A.; Rojas, O. J. Reinforcing Poly(ε-caprolactone) Nanofibers with Cellulose Nanocrystals. *ACS Appl. Mater. Interfaces* **2009**, *1*, 1996−2004.
(53) Paulett, K.; Brayer, W. A.; Hatch, K.; Kalous, T.; Sewell, J.; Liavitskaya, T.; Vyazovkin, S.; Liu, F.; Lukáš, D.; Stanishevsky, A. Effect of nanocrystalline cellulose addition on needleless alternating current electrospinning and properties of nanofibrous polyacrylonitrile meshes. *J. Appl. Polym. Sci.* **2018**, *135*, 45772.
(54) Pirani, S.; Abushammala, H. M. N.; Hashaikeh, R. Preparation and characterization of electrospun PLA/nanocrystalline cellulose-based composites. *J. Appl. Polym. Sci.* **2013**, *130*, 3345−3354.
(55) Piccirillo, G.; Ditaranto, M. V.; Feuerer, N. F. S.; Carvajal Berrio, D. A.; Brauchle, E. M.; Pepe, A.; Bochicchio, B.; Schenke-Layland, K.; Hinderer, S. Non-invasive characterization of hybrid gelatin:poly-l-lactide electrospun scaffolds using second harmonic generation and multiphoton imaging. *J. Mater. Chem. B* **2018**, *6*, 6399−6412.
(56) Colomer, I.; Chamberlain, A.; Haughey, M.; Donohoe, T. Hexafluoroisopropanol as a highly versatile solvent. *Nat. Rev. Chem.* **2017**, *1*, 0088.
(57) Eberson, L.; Hartshorn, M. P.; Persson, O.; Radner, F. Making radical cations live longer. *Chem. Commun.* **1996**, *18*, 2105−2112.
(58) Song, W.; Veiga, D. D.; Custódio, C. A.; Mano, J. F. Bioinspired Degradable Substrates with Extreme Wettability Properties. *Adv. Mater.* **2009**, *21*, 1830−1834.
(59) Wang, S.; Liu, K.; Yao, X.; Jiang, L. Bioinspired Surfaces with Superwettability: New Insight on Theory, Design, and Applications. *Chem. Rev.* **2015**, *115*, 8230−8293.
(60) Novo, L. P.; Bras, J.; García, A.; Belgacem, N.; Curvelo, A. A. S. Subcritical Water: A Method for Green Production of Cellulose Nanocrystals. *ACS Sustainable Chem. Eng.* **2015**, *3*, 2839−2846.
(61) Sisson, K.; Zhang, C.; Farach-Carson, M. C.; Chase, D. B.; Rabolt, J. F. Evaluation of cross-linking methods for electrospun gelatin on cell growth and viability. *Biomacromolecules* **2009**, *10*, 1675−1680.
(62) Auras, R.; Harte, B.; Selke, S. An overview of polylac-tides as packaging materials. *Macromol. Biosci.* **2004**, *4*, 835−864.
(63) Daniel-da-Silva, A. L.; Salgueiro, A. M.; Trindade, T. Effects of Au nanoparticles on thermoresponsive genipin-crosslinked gelatin hydrogels. *Gold Bull.* **2013**, *46*, 25−33.
(64) Barth, A. The infrared absorption of amino acid side chains. *Prog. Biophys. Mol. Biol.* **2000**, *74*, 141−173.
(65) Kim, H.-W.; Yu, H.-S.; Lee, H.-H. Nanofibrous matrices of poly(lactic acid) and gelatin polymeric blends for the improvement of cellular responses. *J. Biomed. Mater. Res., Part A* **2008**, *87*, 25−32.
(66) Cammarata, C. R.; Hughes, M. E.; Ofner, C. M., III Carbodiimide Induced Cross-Linking, Ligand Addition, and Degradation in Gelatin. *Mol. Pharm.* **2015**, *12*, 783−793.
(67) Mengyan, L.; Mondrinos, M. J.; Xuesi, C.; Lelkes, P. I. *2005 IEEE Engineering in Medicine and Biology 27th Annual Conference, Shanghai, China, September*, 2005.
(68) Lee, J.; Tae, G.; Kim, Y. H.; Park, I. S.; Kim, S.-H.; Kim, S. H. The effect of gelatin incorporation into electrospun poly(l-lactide-co-ε-caprolactone) fibers on mechanical properties and cytocompatibility. *Biomaterials* **2008**, *29*, 1872−1879.
(69) Han, B.; Jaurequi, J.; Tang, B. W.; Nimni, M. E. Proanthocyanidin: A natural crosslinking reagent for stabilizing collagen matrices. *J. Biomed. Mater. Res., Part A* **2003**, *65*, 118−124.
(70) Jia, B.; Li, Y.; Yang, B.; Xiao, D.; Zhang, S.; Rajulu, A. V.; Kondo, T.; Zhang, L.; Zhou, J. Effect of microcrystal cellulose and

https://dx.doi.org/10.1021/acsapm.0c00790
ACS Appl. Polym. Mater. 2020, 2, 4836−4847

cellulose whisker on biocompatibility of cellulose-based electrospun scaffolds. *Cellulose* **2013**, *20*, 1911−1923.
(71) Han, J.; Lazarovici, P.; Pomerantz, C.; Chen, X.; Wei, Y.; Lelkes, P. I. Co-Electrospun Blends of PLGA, Gelatin, and Elastin as Potential Nonthrombogenic Scaffolds for Vascular Tissue Engineering. *Biomacromolecules* **2011**, *12*, 399−408.
(72) Heydarkhan-Hagvall, S.; Schenke-Layland, K.; Dhanasopon, A. P.; Rofail, F.; Smith, H.; Wu, B. M.; Shemin, R.; Beygui, R. E.; MacLellan, W. R. Three-dimensional electrospun ECM-based hybrid scaffolds for cardiovascular tissue engineering. *Biomaterials* **2008**, *29*, 2907−2914.
(73) Mele, E. Electrospinning of natural polymers for advanced wound care: towards responsive and adaptive dressings. *J. Mat. Chem. B* **2016**, *4*, 4801−4812.
(74) Thenmozhi, S.; Dharmaraj, N.; Kadirvelu, K.; Kim, H. Y. Electrospun nanofibers: New generation materials for advanced applications. *Mater. Sci. Eng., B* **2017**, *217*, 36−48.
(75) Mo, Y.; Guo, R.; Liu, J.; Lan, Y.; Zhang, Y.; Xue, W.; Zhang, Y. Preparation and properties of PLGA nanofiber membranes reinforced with cellulose nanocrystals. *Colloids Surf., B* **2015**, *132*, 177−184.
(76) Changsarn, S.; Mendez, J. D.; Shanmuganathan, K.; Foster, E. J.; Weder, C.; Supaphol, P. Biologically Inspired Hierarchical Design of Nanocomposites Based on Poly(ethylene oxide) and Cellulose Nanofibers. *Macromol. Rapid Commun.* **2011**, *32*, 1367−1372.
(77) Zhou, C.; Chu, R.; Wu, R.; Wu, Q. Electrospun Polyethylene Oxide/Cellulose Nanocrystal Composite Nanofibrous Mats with Homogeneous and Heterogeneous Microstructures. *Biomacromolecules* **2011**, *12*, 2617−2625.
(78) Swindle-Reilly, K. E.; Paranjape, C. S.; Miller, C. A. Electrospun poly(caprolactone)-elastin scaffolds for pe-ripheral nerve regeneration. *Prog. Biomater.* **2014**, *3*, 20.
(79) Rnjak-Kovacina, J.; Weiss, A. S. Increasing the pore size of electrospun scaffolds. *Tissue Eng., Part B* **2011**, *17*, 365−372.
(80) Ameer, J. M.; Pr, A. K.; Kasoju, N. Strategies to Tune Electrospun Scaffold Porosity for Effective Cell Response in Tissue Engineering. *J. Funct. Biomater.* **2019**, *10*, 30.
(81) Jaiswal, A. K.; Kadam, S. S.; Soni, V. P.; Bellare, J. R. Improved functionalization of electrospun PLLA/gelatin scaffold by alternate soaking method for bone tissue engineering. *Appl. Surf. Sci.* **2013**, *268*, 477−488.
(82) Boral, S.; Gupta, A. N.; Bohidar, H. B. Swelling and de-swelling kinetics of gelatin hydrogels in ethanol−water marginal solvent. *Int. J. Biol. Macromol.* **2006**, *39*, 240−249.
(83) Elishav, O.; Beilin, V.; Rozent, O.; Shter, G. E.; Grader, G. S. Thermal shrinkage of electrospun PVP nanofibers. *J. Polym. Sci., Part B: Polym. Phys.* **2018**, *56*, 248−254.
(84) Saarai, A.; Kasparkova, V.; Sedlacek, T.; Saha, P. *A Comparative Study of Crosslinked Sodium Alginate/Gelatin Hydrogels for Wound Dressing, Wseas International Conference on Energy and Development—Environment—Biomedicine*, 2011; pp 384−389.
(85) Shi, Q.; Zhou, C.; Yue, Y.; Guo, W.; Wu, Y.; Wu, Q. Mechanical properties and in vitro degradation of electrospun bio-nanocomposite mats from PLA and cellulose nanocrystals. *Carbohydr. Polym.* **2012**, *90*, 301−308.
(86) Zhou, C.; Shi, Q.; Guo, W.; Terrell, L.; Qureshi, A. T.; Hayes, D. J.; Wu, Q. Electrospun Bio-Nanocomposite Scaffolds for Bone Tissue Engineering by Cellulose Nanocrystals Reinforcing Maleic Anhydride Grafted PLA. *ACS Appl. Mater. Interfaces* **2013**, *5*, 3847−3854.
(87) Bagheriasl, D.; Carreau, P. J.; Riedl, B.; Dubois, C.; Hamad, W. Y. Shear rheology of polylactide (PLA)-cellulose nanocrystal (CNC) nanocomposites. *Cellulose* **2016**, *23*, 1885−1897.
(88) Kim, G.; Ahn, S.; Kim, Y.; Cho, Y.; Chun, W. Coaxial structured collagen-alginate scaffolds: fabrication, physical properties, and biomedical application for skin tissue regeneration. *J. Mater. Chem.* **2011**, *21*, 6165−6172.
(89) Megret, C.; Lamure, A.; Pieraggi, M. T.; Lacabanne, C.; Guantieri, V.; Tamburro, A. M. Solid-state studies on synthetic fragments and analogues of elastin. *Int. J. Biol. Macromol.* **1993**, *15*, 305−312.
(90) Lim, H.; Hoag, S. W. Plasticizer Effects on Physical-Mechanical Properties of Solvent Cast Soluplus Films. *AAPS PharmSciTech* **2013**, *14*, 903−910.
(91) Hubble, M. A.; Ferrer, A.; Tyagi, P.; Yin, Y.; Salas, C.; Pal, L.; Rojas, O. J. Nanocellulose in Thin Films, Coat-ings, and Plies for Packaging Applications: A Review. *Bioresources* **2017**, *12*, 2143−2233.
(92) Mano, J. F.; Sousa, R. A.; Boesel, L. F.; Neves, N. M.; Reis, R. L. Bioinert, biodegradable and injectable polymeric matrix composites for hard tissue replacement: state of the art and recent developments. *Compos. Sci. Technol.* **2004**, *64*, 789−817.
(93) Kluger, P. J.; Wyrwa, R.; Weisser, J.; Maierle, J.; Votteler, M.; Rode, C.; Schnabelrauch, M.; Walles, H.; Schenke-Layland, K. Electrospun poly(D/L-lactide-co-L-lactide) hybrid matrix: a novel scaffold material for soft tissue engineering. *J. Mater. Sci.: Mater. Med.* **2010**, *21*, 2665−2671.
(94) Mo, Y.; Guo, R.; Liu, J.; Lan, Y.; Zhang, Y.; Xue, W.; Zhang, Y. Preparation and properties of PLGA nanofiber membranes reinforced with cellulose nanocrystals. *Colloids Surf., B* **2015**, *132*, 177−184.
(95) Abudula, T.; Saeed, U.; Memic, A.; Gauthaman, K.; Hussain, M. A.; Al-Turaif, H. Electrospun cellulose Nano fibril reinforced PLA/PBS composite scaffold for vascular tissue engineering. *J. Polym. Res.* **2019**, *26*, 110.
(96) Rahmat, M.; Karrabi, M.; Ghasemi, I.; Zandi, M.; Azizi, H. Silane crosslinking of electrospun poly (lactic acid)/nanocrystalline cellulose bionanocomposite. *Mater. Sci. Eng., C* **2016**, *68*, 397−405.
(97) Hossain, K. M. Z.; Hasan, M. S.; Boyd, D.; Rudd, C. D.; Ahmed, I.; Thielemans, W. Effect of cellulose nanowhiskers on surface morphology, mechanical properties, and cell adhesion of melt-drawn polylactic acid fibers. *Biomacromolecules* **2014**, *15*, 1498−1506.
(98) Pereira, M. M.; Raposo, N. R. B.; Brayner, R.; Teixeira, E. M.; Oliveira, V.; Quintão, C. C. R.; Camargo, L. S. A.; Mattoso, L. H. C.; Brandão, H. M. Cytotoxicity and expression of genes involved in the cellular stress response and apoptosis in mammalian fibroblast exposed to cotton cellulose nanofibers. *Nanotechnology* **2013**, *24*, 075103.
(99) Machado, R.; Da Costa, A.; Sencadas, V.; Garcia-Arévalo, C.; Costa, C. M.; Padrão, J.; Gomes, A.; Lanceros-Méndez, S.; Rodríguez-Cabello, J. C.; Casal, M. Electrospun silk-elastin-like fibre mats for tissue engineering applications. *Biomed. Mater.* **2013**, *8*, 065009.
(100) Hong, N.; Siquan, Z.; Jing, W.; Xiangrong, C.; Tao, L.; Weiyang, W.; Weijuan, Z.; Yun, C. Cellulose nanowhiskers: Preparation, characterization and cytotoxicity evaluation. *Biomed. Mater. Eng.* **2012**, *22*, 121−127.
(101) Koegler, P.; Pasic, P.; Gardiner, J.; Glattauer, V.; Kingshott, P.; Thissen, H. Polymerizable Peptide Copolymer Coatings for the Control of Biointerfacial Interactions. *Biomacromolecules* **2014**, *15*, 2265−2273.
(102) Niamsap, T.; Lam, N. T.; Sukyai, P. Production of hydroxyapatite-bacterial nanocellulose scaffold with assist of cellulose nanocrystals. *Carbohydr. Polym.* **2019**, *205*, 159−166.
(103) Zahedi, P.; Rezaeian, I.; Ranaei-Siadat, S.-O.; Jafari, S.-H.; Supaphol, P. A review on wound dressings with an emphasis on electrospun nanofibrous polymeric bandages. *Polym. Adv. Technol.* **2010**, *21*, 77−95.

https://dx.doi.org/10.1021/acsapm.0c00790
ACS Appl. Polym. Mater. 2020, 2, 4836−4847